

AIAA 96-1664
On Perfectly Matched Layer As An Absorbing Boundary Condition

Fang Q. Hu

Old Dominion University Norfolk, VA

2nd AIAA/CEAS Aeroacoustics Conference May 6-8,1996/State College, PA

On Perfectly Matched Layer As An Absorbing Boundary Condition

 $Fang \ Q. \ Hu^{\dagger}$ Department of Mathematics and Statistics, Old Dominion University Norfolk, VA 23529

ABSTRACT

A Perfectly Absorbing Technique (PAT) is proposed for numerical solutions of the Euler equations. This technique follows the recent studies of Perfectly Matched Layer (PML) as absorbing boundary conditions. In the present paper, we construct the Perfectly Matched Layer equations for linear as well as non-linear Euler equations as an absorbing boundary condition. Plane wave solutions and propagation properties are analyzed for a uniform flow in an arbitrary direction. It is shown that the proposed PML equations are capable of absorbing the out-going acoustic, vorticity and entropy waves at numerical boundaries without reflection (theoretically) for any angle of incidence and frequency of the wave. The absorption rate is also independent of the wave frequency/wavelength. The PML equations are then extended to non-uniform mean flows. Moreover, by introducing a "pseudo mean flow", PML equations for nonlinear Euler equations are constructed. The pseudo mean flow needs not to be an accurate prediction of the actual mean steady flow. Consequently, it becomes possible to apply the PML equations without the exact mean flow being available. Numerical examples that demonstrate the validity of the proposed absorbing boundary conditions are presented.

1. Introduction

Recently, a new technique for absorbing boundary conditions, here referred to as the Perfectly Absorbing Technique (PAT), has been proposed for the Euler equations [1]. This technique follows the recent work on Perfectly Matched Layer (PML) first developed by Berenger for numerical solutions of the Maxwell equations [2]. Numerical examples of ref [1] and those in the present paper indicate that this technique can provide a very effective absorbing boundary condition for computational fluid dynamics and, particularly, computational aeroacoustics where highly accurate numerical boundary condition is essential.

In numerical simulations, the physical domains are often necessarily truncated due to the limitation of a finite

computational domain. At these artificial boundaries, numerical non-reflecting or absorbing boundary conditions are needed so that the out-going waves are not reflected. Various computational techniques have been developed in the past to minimize the reflection of out-going waves. They include the out-flow boundary conditions based on the characteristics of the Euler equations [3, 4] and the radiation boundary conditions based on the far field asymptotic solutions [5, 6, 7, 8, 9], to cite just a few. A recent review can be found in reference [10]. In addition, a buffer zone technique has been developed in which the mean flow is altered gradually to be supersonic in a buffer region adjacent to the artificial boundary [11, 12].

A different approach has been taken in the proposed Perfectly Absorbing Technique. In this approach, a region with a width of a few grid points, called the PML domain, is introduced adjacent to the artificial boundaries, such as the radiation and out-flow boundaries. In the PML domain, Perfectly Matched Layer equations are constructed so that the out-going waves are absorbed without reflection. Thus, in numerical calculations, the computational domain is divided into the interior domain, where the Euler equations are applied, and the PML domains, where the proposed PML equations are applied, as shown in Figure 1. In ref [1], PML equations for the linearized Euler equations with a uniform mean flow were proposed. It was shown that the proposed PML equations are capable of absorbing the out-going acoustic, vorticity and entropy waves without reflection for any angle of incidence and frequency of the The absorption rate is also independent of the wave frequency/wavelength. Thus the effectiveness of the absorbing boundary condition is not affected by a change of frequency or wave number of the out-going waves.

In this paper, we further study the Perfectly Absorbing Technique for non-uniform mean flows and for non-linear Euler equations. In section 2, we first re-examine the theoretical reflection and transmission properties of the PML equations for a mean flow which is in an arbitrary direction. It will be shown, again, that the theoretical reflection coefficients are zero for the linear waves. Then, in Section 3, the PML equations are extended to the linearized Euler equations with a non-uniform mean flow. In Section 4, by introducing a "pseudo mean flow", PML equations for non-linear Euler equations are proposed. Numerical examples are presented in Section 5. Concluding remarks are given in Section 6.

Copyright ©1996 by F. Q. Hu. Published by the American Institute of Aeronautics and Astronautics, Inc. with permission.

[†] Assistant Professor. Member AIAA.

2. Perfectly Matched Layer equations for a uniform mean flow

Consider the two-dimensional linearized Euler equations with a uniform mean flow :

$$\frac{\partial u'}{\partial t} + U_o \frac{\partial u'}{\partial x} + V_o \frac{\partial u'}{\partial y} + \frac{\partial p'}{\partial x} = 0$$
 (1.1)

$$\frac{\partial v'}{\partial t} + U_o \frac{\partial v'}{\partial x} + V_o \frac{\partial v'}{\partial y} + \frac{\partial p'}{\partial y} = 0$$
 (1.2)

$$\frac{\partial p'}{\partial t} + U_o \frac{\partial p'}{\partial x} + V_o \frac{\partial p'}{\partial y} + \left(\frac{\partial u'}{\partial x} + \frac{\partial v'}{\partial y}\right) = 0 \quad (1.3)$$

$$\frac{\partial \rho'}{\partial t} + U_o \frac{\partial \rho'}{\partial x} + V_o \frac{\partial \rho'}{\partial y} + \left(\frac{\partial u'}{\partial x} + \frac{\partial v'}{\partial y}\right) = 0 \quad (1.4)$$

in which u' and v' are the velocity perturbations in the x and y directions respectively, p' is the pressure, and ρ' is the density. Through out this paper, the velocities are non-dimensionalized by the speed of sound a_0 , the density by $\bar{\rho}_0$ and the pressure by $\bar{\rho}_0 a_0^2$, where $\bar{\rho}_0$ is the mean density. U_0 and V_0 are the mean velocities in the x and y directions respectively, i.e.,

$$U_o = M \cos \alpha$$
, $V_o = M \sin \alpha$,

where α is the angle between the direction of mean flow and the x-axis and M is the Mach number. In particular, we will be interested in subsonic flows, i.e., M < 1.

It is well known that the linearized Euler equations (1.1)-(1.4) support acoustic waves, which travel with the speed of sound relative to the mean flow, and vorticity and entropy waves, which travel with the mean flow. Our aim is to define a perfectly matched layer to be used at a region adjacent to the artificial boundary that can absorb the out-going acoustic, vorticity and entropy waves with little or no reflection in computation.

We split the flow variables u', v', p' and ρ' in equations (1.1)-(1.4) into sub-components u_1 , u_2 , v_1 , v_2 , p_1 , p_2 and ρ_1 , ρ_2 and define the following equations for the Perfectly Matched Layer (PML):

$$\frac{\partial u_1}{\partial t} + \sigma_x u_1 = -\frac{\partial (p_1 + p_2)}{\partial x} - U_o \frac{\partial (u_1 + u_2)}{\partial x}$$
 (2.1)

$$\frac{\partial u_2}{\partial t} + \sigma_y u_2 = -V_o \frac{\partial (u_1 + u_2)}{\partial y} \tag{2.2}$$

$$\frac{\partial v_1}{\partial t} + \sigma_y v_1 = -\frac{\partial (p_1 + p_2)}{\partial y} - V_o \frac{\partial (v_1 + v_2)}{\partial y}$$
 (2.3)

$$\frac{\partial v_2}{\partial t} + \sigma_x v_2 = -U_o \frac{\partial (v_1 + v_2)}{\partial x} \tag{2.4}$$

$$\frac{\partial p_1}{\partial t} + \sigma_x p_1 = -\frac{\partial (u_1 + u_2)}{\partial x} - U_o \frac{\partial (p_1 + p_2)}{\partial x}$$
 (2.5)

$$\frac{\partial p_2}{\partial t} + \sigma_y p_2 = -\frac{\partial (v_1 + v_2)}{\partial y} - V_o \frac{\partial (p_1 + p_2)}{\partial y}$$
 (2.6)

$$\frac{\partial \rho_1}{\partial t} + \sigma_x \rho_1 = -\frac{\partial (u_1 + u_2)}{\partial x} - U_o \frac{\partial (\rho_1 + \rho_2)}{\partial x} \quad (2.7)$$

$$\frac{\partial \rho_2}{\partial t} + \sigma_y \rho_2 = -\frac{\partial (v_1 + v_2)}{\partial y} - V_o \frac{\partial (\rho_1 + \rho_2)}{\partial y}$$
 (2.8)

In the above, coefficients σ_x and σ_y have been introduced for the absorption of waves in the layer. They are called absorption coefficients and assumed to be greater than or equal to zero. It is to be noted that, when $\sigma_x = \sigma_y = 0$, equations (2.1)-(2.8) can be reduced to the Euler equations (1.1)-(1.4) with $u' = u_1 + u_2$, $v' = v_1 + v_2$, $p' = p_1 + p_2$ and $\rho' = \rho_1 + \rho_2$. Thus the Euler equations are a special case of the PML equations. Moreover, the spatial derivatives involve only the total u', v', p' and ρ' . Consequently, the implementation of the PML equations in finite difference schemes are quite straightforward.

In introducing PML domains, two kinds of interfaces are created, namely, the interfaces between the interior domain and a PML domain and those between two PML domains, as shown in Figure 2. The former, of course, can be regarded as a special case of the later. At the interfaces, u', v', p' and ρ' are assumed to be continuous. The absorbing coefficients, σ_x and σ_y , will be chosen such that σ_y is the same across an interface normal to x and σ_x is the same normal to y, as in [2]. Since the Euler equations for the interior domain are considered as PML equations with both absorption coefficients being zero, σ_y or σ_x will be consequently zero across an interface normal to x or y between an interior domain and a PML domain. This is as shown in Figure 2. It is important that σ_x and σ_y are "matched" in this way.

If no mean flow is present, i.e., $U_o = V_o = 0$, equations (2.2) and (2.4) may not be used. We also note that, when $V_o = 0$, equations (2.1)-(2.8) are slightly different from those of ref [1], although they are computationally equivalent [18]. The wave reflection and transmission properties will be re-examined below for equations (2.1)-(2.8). In what follows, we show the wave propagation and absorption properties of the PML equations defined above and calculate the reflection and transmission coefficients at an interface between two PML domains.

2.1 Linear waves in the Perfectly Matched Layer

Let a plane wave solution in the PML domain be expressed as

$$[u_1, u_2, v_1, v_2, p_1, p_2, \rho_1, \rho_2]$$

$$= \left[u_{10}, u_{20}, v_{10}, v_{20}, p_{10}, p_{20}, \rho_{10}, \rho_{20}\right] e^{i(k_x x + k_y y - \omega t)} \quad (3$$

in which a subscript 0 has been used to denote the amplitudes of the components. By substituting (3) into (2.1)-(2.8), we get

$$(\omega + i\sigma_x)u_{10} = k_x(p_{10} + p_{20}) + k_xU_o(u_{10} + u_{20})$$
(4.1)

$$(\omega + i\sigma_y)u_{20} = k_y V_o(u_{10} + u_{20}) \tag{4.2}$$

$$(\omega + i\sigma_y)v_{10} = k_y(p_{10} + p_{20}) + k_yV_o(v_{10} + v_{20})$$
 (4.3)

$$(\omega + i\sigma_x)v_{20} = k_x U_o(v_{10} + v_{20}) \tag{4.4}$$

$$(\omega + i\sigma_x)p_{10} = k_x(u_{10} + u_{20}) + k_xU_o(p_{10} + p_{20})$$
(4.5)

$$(\omega + i\sigma_y)p_{20} = k_y(v_{10} + v_{20}) + k_yV_o(p_{10} + p_{20}) \quad (4.6)$$

$$(\omega + i\sigma_x)\rho_{10} = k_x(u_{10} + u_{20}) + k_xU_o(\rho_{10} + \rho_{20}) \quad (4.7)$$

$$(\omega + i\sigma_y)\rho_{20} = k_y(v_{10} + v_{20}) + k_yV_o(\rho_{10} + \rho_{20}) \quad (4.8)$$

For convenience of discussion, let

$$u_0 = u_{10} + u_{20}, \ v_0 = v_{10} + v_{20},$$
 (5)

and denote

$$D \equiv (\omega - k_x U_o + i\sigma_x)(\omega - k_y V_o + i\sigma_y) - k_x k_y U_o V_o.$$
 (6)

It will be shown below that equations (4.1)-(4.8) support acoustic waves, when $D \neq 0$, and vorticity and entropy waves, when D = 0.

2.1.1 Acoustic Waves

When $D \neq 0$, it is easy to find that the amplitudes of the wave components in (3) can be expressed in terms of u_0 and v_0 as follows:

$$u_{10} = \frac{\omega - k_y V_o + i\sigma_y}{\omega + i\sigma_y} u_0 \tag{7.1}$$

$$v_{10} = \frac{\omega - k_x U_o + i\sigma_x}{\omega + i\sigma_x} v_0 \tag{7.2}$$

$$u_{20} = \frac{k_y V_o}{\omega + i\sigma_y} u_0 \tag{7.3}$$

$$v_{20} = \frac{k_x U_o}{\omega + i\sigma_x} v_0 \tag{7.4}$$

$$p_{10} = \frac{k_x(\omega - k_y V_o + i\sigma_y) u_0 + k_x k_y U_o v_0}{D}$$
 (7.5)

$$p_{20} = \frac{k_y(\omega - k_x U_o + i\sigma_x) v_0 + k_y k_x V_o u_0}{D}$$
 (7.6)

$$\rho_{10} = \frac{k_x(\omega - k_y V_o + i\sigma_y) u_0 + k_x k_y U_o v_0}{D}$$

$$\rho_{20} = \frac{k_y(\omega - k_x U_o + i\sigma_x) v_0 + k_y k_x V_o u_0}{D}$$
(7.8)

$$\rho_{20} = \frac{k_y(\omega - k_x U_o + i\sigma_x) v_0 + k_y k_x V_o u_0}{D}$$
 (7.8)

In addition, by (4.1) and (4.3), we have

$$\frac{(\omega + i\sigma_x) u_{10} - k_x U_o u_0}{(\omega + i\sigma_y) v_{10} - k_y V_o v_0} = \frac{k_x}{k_y}.$$

Using (7.1) and (7.2), the above gives

$$\frac{\omega + i\sigma_x}{\omega + i\sigma_y} \frac{u_0}{v_0} = \frac{k_x}{k_y}.$$
 (8)

By substituting (7.1)-(7.6) into (4.1) and (4.3), we get

$$\frac{(\omega + i\sigma_x)(\omega - k_y V_o + i\sigma_y)}{\omega + i\sigma_y} u_0$$

$$= \frac{k_x^2(\omega + i\sigma_y)u_0 + k_x k_y(\omega + i\sigma_x)v_0}{D} + k_x U_o u_0 \qquad (9.1)$$

$$\frac{(\omega + i\sigma_y)(\omega - k_x U_o + i\sigma_x)}{\omega + i\sigma_x}v_0$$

$$=\frac{k_x k_y (\omega + i\sigma_y) u_0 + k_y^2 (\omega + i\sigma_x) v_0}{D} + k_y V_o v_0 \qquad (9.2)$$

respectively. This yields a homogeneous system for u_0 and v_0 . For (9.1) and (9.2) to have non-trivial solutions, it is found that the following dispersion relation for k_x , k_y and ω has to hold:

$$\left[(\omega + i\sigma_x)(\omega + i\sigma_y) - k_x U_o(\omega + i\sigma_y) - k_y V_o(\omega + i\sigma_x) \right]^2$$

$$-k_x^2(\omega + i\sigma_y)^2 - k_y^2(\omega + i\sigma_x)^2 = 0.$$
 (10)

However, it has been found more convenient to express k_x and k_y in terms of u_0 and v_0 . Upon eliminating k_y and k_x in the numerators of (9.1) and (9.2), respectively, using equation (8), we obtain

$$k_x = \pm \frac{D}{\omega + i\sigma_y} \frac{u_0}{\sqrt{u_0^2 + v_0^2}},$$
 (11.1)

$$k_y = \pm \frac{D}{\omega + i\sigma_x} \frac{v_0}{\sqrt{u_0^2 + v_0^2}}$$
 (11.2)

The positive and negative signs indicate the direction of wave propagation. The positive sign will be taken in the discussions followed. For convenience, we express u_0 and v_0 as

$$u_0 = A\cos\phi,\tag{12.1}$$

$$v_0 = A\sin\phi. \tag{12.2}$$

The amplitude A and angle ϕ are complex in general. However, as will be seen later, the wave angles are conserved at interfaces. Since ϕ is real for solutions of the Euler equations in the interior domain, it would remain real in the PML domains as well.

By substituting (12.1)-(12.2) into (11.1)-(11.2) and solving for k_x and k_y , we get

$$k_x = \frac{\omega + i\sigma_x}{1 + U_0 \cos\phi + V_0 \sin\phi} \cos\phi, \qquad (13.1)$$

$$k_x = \frac{\omega + i\sigma_x}{1 + U_o \cos \phi + V_o \sin \phi} \cos \phi, \qquad (13.1)$$

$$k_y = \frac{\omega + i\sigma_y}{1 + U_o \cos \phi + V_o \sin \phi} \sin \phi. \qquad (13.2)$$

Then, it follows that the plane wave solution to (4.1)-(4.8)can be expressed as follows:

$$\begin{pmatrix} u_1 \\ u_2 \\ v_1 \\ v_2 \\ p_1 \\ p_2 \\ \rho_1 \\ \rho_2 \end{pmatrix} = \frac{A}{1 + U_o \cos \phi + V_o \sin \phi} \begin{pmatrix} (1 + U_o \cos \phi) \cos \phi \\ V_o \sin \phi \cos \phi \\ (1 + V_o \sin \phi) \sin \phi \\ U_o \cos \phi \sin \phi \\ (\cos \phi + U_o) \cos \phi \\ (\sin \phi + V_o) \sin \phi \\ (\cos \phi + U_o) \cos \phi \\ (\sin \phi + V_o) \sin \phi \end{pmatrix}$$

$$\times e^{i\omega(\frac{(\cos\phi)x+(\sin\phi)y}{1+U_0\cos\phi+V_0\sin\phi}-t)}e^{-\frac{\sigma_x(\cos\phi)x+\sigma_y(\sin\phi)y}{1+U_0\cos\phi+V_0\sin\phi}}.$$
 (14)

It is easy to see that the first exponential function of the above expression represents a wave propagating with the speed of sound (which is unity in the non-dimensional variables) relative to the mean flow in the direction making an angle ϕ with respect to the x-axis [13]. This solution, thus, represents the acoustic wave in the PML domain. Furthermore, when σ_x or σ_y is not zero, the magnitude of the wave decreases exponentially as it propagates in the xor y direction respectively. We point out also that the rate of absorption in (14) is independent of the frequency.

2.1.2 Vorticity Waves

When D = 0, it can be shown that the plane wave solutions of (4.1)-(4.8) represent the vorticity and entropy waves in the PML domain, as it follows easily from (4.1) and (4.2) that $p_{10} + p_{20} = 0$. The amplitudes of each components in (3) can now be expressed in terms of u_0 , v_0 and ρ_0 where $\rho_0 = \rho_{10} + \rho_{20}$. We will consider the vorticity and entropy waves separately. For vorticity waves, we let $\rho_0 = 0$ and, for convenience, denote u_0 and v_0 as

$$u_0 = -B\sin\psi,\tag{15.1}$$

$$v_0 = B\cos\psi. \tag{15.2}$$

Then, it follows from (4.1)-(4.8) that

$$k_x = \frac{(\omega + i\sigma_x)\cos\psi}{U_o\cos\psi + V_o\sin\psi},$$

$$k_y = \frac{(\omega + i\sigma_y)\sin\psi}{U_o\cos\psi + V_o\sin\psi}.$$
(16.1)

$$k_y = \frac{(\omega + i\sigma_y)\sin\psi}{U_0\cos\psi + V_0\sin\psi}.$$
 (16.2)

The plane wave solution to (4.1)-(4.8) can now be expressed as

$$\begin{pmatrix} u_1 \\ u_2 \\ v_1 \\ v_2 \\ p_1 \\ p_2 \\ \rho_1 \\ \rho_2 \end{pmatrix} = \frac{B}{U_o \cos \psi + V_o \sin \psi} \begin{pmatrix} -U_o \cos \psi \sin \psi \\ -V_o \sin^2 \psi \\ V_o \sin \psi \cos \psi \\ U_o \cos^2 \psi \\ -\cos \psi \sin \psi \\ \sin \psi \cos \psi \\ -\cos \psi \sin \psi \\ \sin \psi \cos \psi \end{pmatrix}$$

$$\times e^{i\omega(\frac{(\cos\psi)x + (\sin\psi)y}{U_0\cos\psi + V_0\sin\psi} - t)} e^{-\frac{\sigma_x(\cos\psi)x + \sigma_y(\sin\psi)y}{U_0\cos\psi + V_0\sin\psi}}.$$
 (17)

It is easy to verify that the first exponential function of the above expression represents a plane wave that is propagating with the mean flow (U_o,V_o) . (It satisfies the convection equation $\frac{\partial f}{\partial t} + U_o \frac{\partial f}{\partial x} + V_o \frac{\partial f}{\partial y} = 0$). Furthermore, the wave amplitudes are decreased exponentially when σ_x or σ_y is not zero.

2.1.3 Entropy Waves

For entropy waves, we let $u_0 = v_0 = 0$ and $\rho_0 = C$. Then, the plane wave solution having an angle Ψ with the x-axis is

$$\begin{bmatrix} \frac{d_2}{v_1} \\ v_2 \\ p_1 \\ p_2 \\ \rho_1 \\ \rho_2 \end{bmatrix} = \frac{C}{U_o \cos \Psi + V_o \sin \Psi} \begin{bmatrix} 0 \\ 0 \\ 0 \\ 0 \\ 0 \\ U_o \cos \Psi \\ V_o \sin \Psi \end{bmatrix}$$

$$\times e^{i\omega(\frac{U_o\cos\Psi+V_o\sin\Psi}{-t})}e^{-\frac{U_o\cos\Psi+V_o\sin\Psi}{-t}}.$$
 (18)

This solution represents the entropy wave in the PML domain. It travels with the mean flow and decays exponentially when σ_x or σ_y is not zero.

2.2 Reflection and transmission at interfaces between two Perfectly Matched Layers

We now consider wave reflection and transmission at an interface between two PML domains. This, of course, includes the interface between the interior domain and a PML domain for the reason stated previously. The absorbing coefficients, σ_x and σ_y , are assigned such that σ_y is the same across an interface normal to x and σ_x is the same normal to y. In what follows we show that the reflection coefficient at an interface downstream normal to x is zero for incident acoustic, vorticity and entropy waves. Similar results can be established analogously for other interfaces.

Let the interface be located downstream at x = 0and the absorption coefficients be σ_{x1} and σ_y on one side and σ_{x2} and σ_y on the other (Figure 3). Suppose that the incident acoustic, vorticity and entropy waves have amplitudes A_i , B_i , C_i and angles ϕ_i , ψ_i , Ψ_i , respectively, then, for a subsonic mean flow, the possible reflection at a downstream boundary is an upstream traveling acoustic wave. Clearly, it is sufficient to consider the case when the three incident waves have the same wavenumber in the y direction. Otherwise, they can be considered separately. Then, by the results of previous section, the incident, reflected and transmitted waves can be expressed as follows: (a) Incident waves:

$$\begin{pmatrix} u_1 \\ u_2 \\ v_1 \\ v_2 \\ p_1 \\ p_2 \\ \rho_1 \\ \rho_2 \end{pmatrix} = \frac{A_i}{1 + U_o \cos \phi_i + V_o \sin \phi_i} \begin{pmatrix} (1 + U_o \cos \phi_i) \cos \phi_i \\ V_o \sin \phi_i \cos \phi_i \\ (1 + V_o \sin \phi_i) \sin \phi_i \\ U_o \cos \phi_i \sin \phi_i \\ (\cos \phi_i + U_o) \cos \phi_i \\ (\sin \phi_i + V_o) \sin \phi_i \\ (\cos \phi_i + U_o) \cos \phi_i \\ (\sin \phi_i + V_o) \sin \phi_i \end{pmatrix}$$

$$\times e^{i\omega\left(\frac{(\cos\phi_i)x + (\sin\phi_i)y}{1 + U_0\cos\phi_i + V_0\sin\phi_i} - t\right)} e^{-\frac{\sigma_{x1}(\cos\phi_i)x + \sigma_y(\sin\phi_i)y}{1 + U_0\cos\phi_i + V_0\sin\phi_i}}$$

$$+\frac{B_{i}}{U_{o}\cos\psi_{i}+V_{o}\sin\psi_{i}}\begin{pmatrix} -U_{o}\cos\psi_{i}\sin\psi_{i}\\ -V_{o}\sin^{2}\psi_{i}\\ V_{o}\sin\psi_{i}\cos\psi_{i}\\ U_{o}\cos^{2}\psi_{i}\\ -\cos\psi_{i}\sin\psi_{i}\\ \sin\psi_{i}\cos\psi_{i}\\ -\cos\psi_{i}\sin\psi_{i}\\ \sin\psi_{i}\cos\psi_{i} \end{pmatrix}$$

$$\times e^{i\omega\left(\frac{(\cos\psi_i)\,x + (\sin\psi_i)\,y}{U_O\cos\psi_i + V_O\sin\psi_i} - t\right)} e^{-\frac{\sigma_{x1}(\cos\psi_i)\,x + \sigma_y(\sin\psi_i)\,y}{U_O\cos\psi_i + V_O\sin\psi_i}}$$

$$+rac{C_i}{U_o\cos\Psi_i+V_o\sin\Psi_i} egin{pmatrix} 0\\0\\0\\0\\0\\U_o\cos\Psi_i\\V_o\sin\Psi_i \end{pmatrix}$$

$$\times e^{i\omega(\frac{(\cos\Psi_i)x + (\sin\Psi_i)y}{U_o\cos\Psi_i + V_o\sin\Psi_i} - t)} e^{-\frac{\sigma_{x1}(\cos\Psi_i)x + \sigma_y(\sin\Psi_i)y}{U_o\cos\Psi_i + V_o\sin\Psi_i}}.$$
 (19.1)

(b) Reflected wave :

$$\begin{pmatrix} u_1 \\ u_2 \\ v_1 \\ v_2 \\ p_1 \\ p_2 \\ \rho_1 \\ \rho_2 \end{pmatrix} = \frac{A_r}{1 - U_o \cos \phi_r + V_o \sin \phi_r} \begin{pmatrix} (1 - U_o \cos \phi_r) \cos \phi_r \\ -V_o \sin \phi_r \cos \phi_r \\ (1 + V_o \sin \phi_r) \sin \phi_r \\ -U_o \cos \phi_r \sin \phi_r \\ (\cos \phi_r - U_o) \cos \phi_r \\ (\sin \phi_r + V_o) \sin \phi_r \end{pmatrix}$$

$$\times e^{i\omega\left(\frac{-(\cos\phi_r)\,x+(\sin\phi_r)\,y}{1-U_o\cos\phi_r+V_o\sin\phi_r}-t\right)}\,e^{\frac{\sigma_{x_1}(\cos\phi_r)\,x-\sigma_y(\sin\phi_r)\,y}{1-U_o\cos\phi_r+V_o\sin\phi_r}}\;.\eqno(19.2)$$

(c) Transmitted waves:

$$\begin{pmatrix} u_1 \\ u_2 \\ v_1 \\ v_2 \\ p_1 \\ p_2 \\ \rho_1 \\ \rho_2 \end{pmatrix} = \frac{A_t}{1 + U_o \cos \phi_t + V_o \sin \phi_t} \begin{pmatrix} (1 + U_o \cos \phi_t) \cos \phi_t \\ V_o \sin \phi_t \cos \phi_t \\ (1 + V_o \sin \phi_t) \sin \phi_t \\ U_o \cos \phi_t \sin \phi_t \\ (\cos \phi_t + U_o) \cos \phi_t \\ (\sin \phi_t + V_o) \sin \phi_t \end{pmatrix}$$

$$\times e^{i\omega(\frac{(\cos\phi_t)\,x+(\sin\phi_t)\,y}{1+U_o\,\cos\phi_t+V_o\,\sin\phi_t}-t)}\,e^{-\frac{\sigma_{x2}(\cos\phi_t)\,x+\sigma_y(\sin\phi_t)\,y}{1+U_o\,\cos\phi_t+V_o\,\sin\phi_t}}$$

$$+\frac{B_t}{U_o \cos \psi_t + V_o \sin \psi_t} \begin{pmatrix} -U_o \cos \psi_t \sin \psi_t \\ -V_o \sin^2 \psi_t \\ V_o \sin \psi_t \cos \psi_t \\ U_o \cos^2 \psi_t \\ -\cos \psi_t \sin \psi_t \\ \sin \psi_t \cos \psi_t \\ -\cos \psi_t \sin \psi_t \\ \sin \psi_t \cos \psi_t \end{pmatrix}$$

$$\times e^{i\omega(\frac{(\cos\psi_t)\,x+(\sin\psi_t)\,y}{U_o\,\cos\psi_t+V_o\,\sin\psi_t}-t)}\,e^{-\frac{\sigma_{x2}(\cos\psi_t)\,x+\sigma_y(\sin\psi_t)\,y}{U_o\,\cos\psi_t+V_o\,\sin\psi_t}}$$

$$+rac{C_t}{U_o\cos\Psi_t+V_o\sin\Psi_t} egin{pmatrix} 0 \ 0 \ 0 \ 0 \ 0 \ 0 \ U_o\cos\Psi_t \ V_o\sin\Psi_t \end{pmatrix}$$

$$\times e^{i\omega\left(\frac{(\cos\Psi_t)x + (\sin\Psi_t)y}{U_o\cos\Psi_t + V_o\sin\Psi_t} - t\right)} e^{-\frac{\sigma_{x2}(\cos\Psi_t)x + \sigma_y(\sin\Psi_t)y}{U_o\cos\Psi_t + V_o\sin\Psi_t}}. \tag{19.3}$$

The angles of the acoustic waves are as indicated in Figure 3.

At the interface, we impose the condition that $u_1 + u_2$, $v_1 + v_2$, $p_1 + p_2$ and $\rho_1 + \rho_2$ be continuous. Since this continuity is true for all values of y along the interface, it follows that the coefficients of y in the exponents of (19.1)-(19.3) must be the same for all the incident, reflected and transmitted waves. This yields, for the angles of the reflected and transmitted waves,

$$\frac{\sin\phi_r}{1 - U_o\cos\phi_r + V_o\sin\phi_r} = \frac{\sin\phi_i}{1 + U_o\cos\phi_i + V_o\sin\phi_i},$$
(20.1)

$$\frac{\sin \phi_t}{1 + U_o \cos \phi_t + V_o \sin \phi_t} = \frac{\sin \phi_i}{1 + U_o \cos \phi_i + V_o \sin \phi_i},$$
(20.2)

$$\frac{\sin \psi_t}{U_o \cos \psi_t + V_o \sin \psi_t} = \frac{\sin \psi_i}{U_o \cos \psi_i + V_o \sin \psi_i}, \quad (20.3)$$

$$\frac{\sin \Psi_t}{U_o \cos \Psi_t + V_o \sin \Psi_t} = \frac{\sin \Psi_i}{U_o \cos \Psi_i + V_o \sin \Psi_i}.$$
 (20.4)

Solving these equations, it is found that

$$\phi_r = \tan^{-1} \left(\frac{1 - U_o}{1 + U_o} \tan \phi_i \right) ,$$
 (21.1)

$$\phi_t = \phi_i \,, \tag{21.2}$$

$$\psi_t = \psi_i \,, \tag{21.3}$$

$$\Psi_t = \Psi_i \,. \tag{21.4}$$

Moreover, by the continuity of $u_1 + u_2$, $v_1 + v_2$, $p_1 + p_2$ and $\rho_1 + \rho_2$ on both sides of x = 0, we get

$$A_i \cos \phi_i - A_r \cos \phi_r - B_i \sin \psi_i = A_t \cos \phi_t - B_t \sin \psi_t,$$
(22.1)

$$A_i \sin \phi_i + A_r \sin \phi_r + B_i \cos \psi_i = A_t \sin \phi_t - B_t \cos \psi_t,$$
(22.2)

$$A_i + A_r = A_t \,, \tag{22.3}$$

$$A_i + A_r + C_i = A_t + C_t. (22.4)$$

It is straightforward to verify that the only solution to the above equations for any angle of incidence is

$$A_r = 0, (23.1)$$

$$A_t = A_t, (23.2)$$

$$B_t = B_i, (23.3)$$

$$C_t = C_i. (23.4)$$

Therefore, equations (21.1)-(21.4) and (23.1)-(23.4)demonstrate that at an interface between two PML domains downstream normal to the x-axis with absorption coefficients being (σ_{x1}, σ_y) and (σ_{x2}, σ_y) respectively, the reflection is null and the transmitted waves maintain the same direction and amplitude as the incident waves at the interface. This has been shown to be independent of the angle of incidence and frequency of the waves.

The PML equations (2.1)-(2.8) result from separating the spatial derivative terms of the Euler equations such that each equation contains only the derivative with respect to one space variable. This has been shown to give perfectly absorbing equations. This technique of separating spatial derivatives will be extended to the linearized Euler equations with a non-uniform mean flow in Section 3 and, with modifications, to the non-linear Euler equations in Section 4.

2.3 Absorption factor and boundary conditions at the end of a PML domain

We now estimate the rate of wave absorption in actual computation based on the wave forms given in previous discussions. With finite difference schemes, particularly with high-order schemes using wide stencils, the absorption coefficient, i.e., σ_x or σ_y , is usually varied gradually in the PML domain [1,2]. In the present paper, the following form has been used for the variation of σ_x and σ_y :

$$\sigma = \sigma_m \left(\frac{d}{D}\right)^{\beta} \,, \tag{24}$$

where D is the width of the PML domain, d is the distance from its interface with the interior domain and σ_m is the maximum value of σ . Alternatively, the PML domain can also be viewed as consisting of layers with constant σ which varies discretely.

At the end of a PML domain, certain boundary conditions still need to be specified, such as a solid wall type condition or some other radiation conditions. In the present paper, unless otherwise noted, a solid wall boundary condition is applied at the end of the PML domain, i.e., the normal velocity components are set to be zero. Normally, the variables are already quite small at the end of the PML domain after an exponential decay. Suppose the waves are completely reflected at the end of the PML domain,

then the total absorption factor when a wave re-enters the interior domain can be estimated to be

$$e^{-\frac{\sigma_{II}D}{\beta+1}\left(\frac{\cos\phi_{i}}{1+U_{o}\cos\phi_{i}+V_{o}\sin\phi_{i}}+\frac{\cos\phi_{r}}{1-U_{o}\cos\phi_{r}+V_{o}\sin\phi_{r}}\right)}$$
 (25)

for the out-going acoustic waves through layers normal to x. For the vorticity and entropy waves, this factor is

$$e^{-\frac{\sigma_{m}D}{\beta+1}\left(\frac{\cos\psi_{i}}{U_{o}\cos\psi_{i}+V_{o}\sin\psi_{i}}+\frac{\cos\phi_{r}}{1-U_{o}\cos\phi_{r}+V_{o}\sin\phi_{r}}\right)},$$
 (26)

assuming the reflected wave is a upstream-traveling acoustic wave. Clearly, absorption factors are independent of the frequency. They are, however, dependent on the wave angles. There will be, for instance, little absorption in a layer normal to the x-axis if the wave angle is close to $\pm \pi/2$. In actual computation, this does not present a problem as these waves are absorbed by the layers normal to the y-axis

The parameters of the PML domains can thus be adjusted for desired absorption. They can also be determined independent of the size of the interior domain. Experiences show that a value of $\sigma_m D/(\beta+1) \approx 8$ would give satisfactory results. Typically, with a uniform grid of spacing Δx , if $D = 10\Delta x$ and $\beta = 2$, it gives $\sigma_m \Delta x = 2.4$.

The maximum value of σ , however, will be restricted by the stability limit of the time integration scheme used, since an absorption term has been introduced in the PML equations. Detailed considerations are given in the Appendix.

3. Perfectly Matched Layer equations for a non-uniform mean flow

The above PML equations can be extended to the linearized Euler equations with a non-uniform flow. Let the non-dimensionalized equations be written as follows:

$$\frac{\partial u'}{\partial t} + \bar{U}\frac{\partial u'}{\partial x} + \bar{V}\frac{\partial u'}{\partial y} + \frac{1}{\bar{\rho}}\frac{\partial p'}{\partial x} = -\bar{U}_x u' - \bar{U}_y v' + \frac{\bar{P}_x}{\bar{\rho}^2}\rho'$$

$$\frac{\partial v'}{\partial t} + \bar{U}\frac{\partial v'}{\partial x} + \bar{V}\frac{\partial v'}{\partial y} + \frac{1}{\bar{\rho}}\frac{\partial p'}{\partial y} = -\bar{V}_x u' - \bar{V}_y v' + \frac{\bar{P}_y}{\bar{\rho}^2}\rho'$$
(27.1)

$$\frac{\partial p'}{\partial t} + \bar{U}\frac{\partial p'}{\partial x} + \bar{V}\frac{\partial p'}{\partial y} + \gamma \bar{P}\left(\frac{\partial u'}{\partial x} + \frac{\partial v'}{\partial y}\right)
= -\bar{P}_x u' - \bar{P}_y v' - \gamma (\bar{U}_x + \bar{V}_y)p'
\frac{\partial \rho'}{\partial t} + \bar{U}\frac{\partial \rho'}{\partial x} + \bar{V}\frac{\partial \rho'}{\partial y} + \bar{\rho}\left(\frac{\partial u'}{\partial x} + \frac{\partial v'}{\partial y}\right)
= -\bar{\rho}_x u' - \bar{\rho}_y v' - (\bar{U}_x + \bar{V}_y)\rho'$$
(27.4)

(27.4)

where $\bar{U},\ \bar{V},\ \bar{P}$ and $\bar{\rho}$ are the mean velocities, pressure and density, respectively, and the subscripts x and y denote partial derivatives.

Again, we split the variables in the PML domain and define Perfectly Matched Layer equations as follows:

$$\frac{\partial u_1}{\partial t} + \sigma_x u_1 = -\frac{1}{\bar{\rho}} \frac{\partial p'}{\partial x} - \bar{U} \frac{\partial u'}{\partial x} - \bar{U}_x u' + \frac{\bar{P}_x}{\bar{\rho}^2} \rho' \quad (28.1)$$

$$\frac{\partial u_2}{\partial t} + \sigma_y u_2 = -\bar{V} \frac{\partial u'}{\partial y} - \bar{U}_y v' \tag{28.2}$$

$$\frac{\partial v_1}{\partial t} + \sigma_y v_1 = -\frac{1}{\bar{\rho}} \frac{\partial p'}{\partial y} - \bar{V} \frac{\partial v'}{\partial y} - \bar{V}_y v' + \frac{\bar{P}_y}{\bar{\rho}^2} \rho' \quad (28.3)$$

$$\frac{\partial v_2}{\partial t} + \sigma_x v_2 = -\bar{U} \frac{\partial v'}{\partial r} - \bar{V}_x u' \tag{28.4}$$

$$\frac{\partial p_1}{\partial t} + \sigma_x p_1 = -\gamma \bar{P} \frac{\partial u'}{\partial x} - \bar{U} \frac{\partial p'}{\partial x} - \bar{P}_x u' - \gamma \bar{U}_x p'(28.5)$$

$$\frac{\partial p_2}{\partial t} + \sigma_y p_2 = -\gamma \bar{P} \frac{\partial v'}{\partial y} - \bar{V} \frac{\partial p'}{\partial y} - \bar{P}_y v' - \gamma \bar{V}_y p' (28.6)$$

$$\frac{\partial \rho_1}{\partial t} + \sigma_x \rho_1 = -\bar{\rho} \frac{\partial u'}{\partial x} - \bar{U} \frac{\partial \rho'}{\partial x} - \bar{\rho}_x u' - \bar{U}_x \rho' \qquad (28.7)$$

$$\frac{\partial \rho_2}{\partial t} + \sigma_y \rho_2 = -\bar{\rho} \frac{\partial v'}{\partial y} - \bar{V} \frac{\partial \rho'}{\partial y} - \bar{\rho}_y v' - \bar{V}_y \rho' \qquad (28.8)$$

in which $u'=u_1+u_2$, $v'=v_1+v_2$, $p'=p_1+p_2$ and $\rho'=\rho_1+\rho_2$. If the mean flow is uniform, the above reduces to (2.1)-(2.8). The absorption coefficients σ_x and σ_y are chosen in the same way as those in the previous section, i.e., σ_x is the same across an interface normal to the y-axis and σ_y is the same across an interface normal to the x-axis. As indicated by numerical examples in Section 5, the use of above equations in the PML domains leads to very little reflection of out-going waves in a non-uniform mean flow.

4. Perfectly Matched Layer equations for non-linear Euler Equations

We now consider the application of Perfectly Absorbing Technique to the non-linear Euler equations. Previously, most non-reflecting boundary conditions for non-linear Euler equations are based on the assumptions that the boundaries are placed at the far-field and flow perturbations are small. In such cases, i.e., when the equations can be linearized at the boundary and the mean flow is known, the linear PML equations of the previous section can be readily used.

However, often the mean flow at the boundary is not known at the start of the computation or the flow fluctuations are not small so the equations cannot be linearized. In this section, we construct the Perfectly Matched Layer equations for the non-linear Euler equations.

4.1 Pseudo mean flow and PML equations

Let the non-linear Euler equations be written as

$$\frac{\partial u}{\partial t} + u \frac{\partial u}{\partial x} + v \frac{\partial u}{\partial y} + \frac{1}{\rho} \frac{\partial p}{\partial x} = 0$$
 (29.1)

$$\frac{\partial v}{\partial t} + u \frac{\partial v}{\partial x} + v \frac{\partial v}{\partial y} + \frac{1}{\rho} \frac{\partial p}{\partial y} = 0$$
 (29.1)

$$\frac{\partial p}{\partial t} + u \frac{\partial p}{\partial x} + v \frac{\partial p}{\partial y} + \gamma p \left(\frac{\partial u}{\partial x} + \frac{\partial v}{\partial y} \right) = 0 \qquad (29.3)$$

$$\frac{\partial \rho}{\partial t} + u \frac{\partial \rho}{\partial x} + v \frac{\partial \rho}{\partial y} + \rho \left(\frac{\partial u}{\partial x} + \frac{\partial v}{\partial y} \right) = 0 \qquad (29.4)$$

To absorb the out-going waves, we express the variables in the PML domains as

$$u = \tilde{U} + u_1 + u_2 \,, \tag{30.1}$$

$$v = \tilde{V} + v_1 + v_2 \,, \tag{30.2}$$

$$p = \tilde{P} + p_1 + p_2 \,, \tag{30.3}$$

$$\rho = \tilde{\rho} + \rho_1 + \rho_2 \,, \tag{30.4}$$

where \tilde{U} , \tilde{V} , \tilde{P} and $\tilde{\rho}$ represent a time-independent "pseudo mean flow". This pseudo mean flow needs not to be an accurate prediction of the actual mean flow for the problem at hand, but only resembles the actual flow. As will be seen below, it is preferable that it satisfies the steady Euler equations itself. For steady flow solutions, the pseudo mean flow can be updated later in the calculation as time marching proceeds, as described later. Usually, it will be quite easy to obtain a pseudo mean flow that resembles the problem at hand. For instance, a parallel flow profile will satisfy the steady Euler equations and thus can serve as a pseudo mean flow for problems such as mixing layers and jets. In an example given later in this paper, a steady point source solution will serve as a pseudo mean flow for a problem with four out-flow boundaries.

We propose the following Perfectly Matched Layer equations:

$$\frac{\partial u_1}{\partial t} + \sigma_x u_1 = -\frac{1}{\rho} \frac{\partial p}{\partial x} - u \frac{\partial u}{\partial x} + \frac{1}{\tilde{\rho}} \tilde{P}_x + \tilde{U} \tilde{U}_x \quad (31.1)$$

$$\frac{\partial u_2}{\partial t} + \sigma_y u_2 = -v \frac{\partial u}{\partial y} + \tilde{V} \tilde{U}_y \tag{31.2}$$

$$\frac{\partial v_1}{\partial t} + \sigma_y v_1 = -\frac{1}{\rho} \frac{\partial p}{\partial u} - v \frac{\partial v}{\partial u} + \frac{1}{\tilde{\rho}} \tilde{P}_y + \tilde{V} \tilde{V}_y \qquad (31.3)$$

$$\frac{\partial v_2}{\partial t} + \sigma_x v_2 = -u \frac{\partial v}{\partial x} + \tilde{U} \tilde{V}_x \tag{31.4}$$

$$\frac{\partial p_1}{\partial t} + \sigma_x p_1 = -\gamma p \frac{\partial u}{\partial x} - u \frac{\partial p}{\partial x} + \gamma \tilde{P} \tilde{U}_x + \tilde{U} \tilde{P}_x \quad (31.5)$$

$$\frac{\partial p}{\partial t} + \sigma_y p_2 = -\gamma p \frac{\partial v}{\partial y} - v \frac{\partial p}{\partial y} + \gamma \tilde{P} \tilde{V}_y + \tilde{V} \tilde{P}_y \quad (31.6)$$

$$\frac{\partial \rho_1}{\partial t} + \sigma_x \rho_1 = -\rho \frac{\partial u}{\partial x} - u \frac{\partial \rho}{\partial x} + \tilde{\rho} \tilde{U}_x + \tilde{U} \tilde{\rho}_x \qquad (31.7)$$

$$\frac{\partial \rho_2}{\partial t} + \sigma_y \rho_2 = -\rho \frac{\partial v}{\partial y} - v \frac{\partial \rho}{\partial y} + \tilde{\rho} \tilde{V}_y + \tilde{V} \tilde{\rho}_y$$
 (31.8)

Here, subscripts x and y have been used to denote the partial derivatives of the pseudo mean flow.

It is easy to see that equations (31.1)-(31.8) can be reduced to the non-linear Euler equations (29.1)-(29.4) when $\sigma_x = \sigma_y = 0$ by adding the split equations, provided that the time-independent pseudo mean flow itself satisfies the steady Euler equations. It is also to be noted that, upon linearization, they reduce to the linear PML equations

given in (28.1)-(28.8). Furthermore, the spatial derivatives involve the total u, v, p and ρ only. This leads to easy implementation in spatial discretization.

Since the variables in the PML domain decay exponentially and are nearly zero at the end of a PML domain, as discussed in Section 2.3, adding the pseudo mean flow terms in (31.1)-(31.8) makes the PML equations consistent. As a result, by applying these equations, the differences between the actual and the pseudo "mean" values are absorbed and reduced exponentially in the PML domain. Numerical results indicate that the use of (31.1)-(31.8) leads to very little reflection even when the out-going waves are not linear. We expect that their use will also accelerate convergence to steady state in aerodynamic computations.

4.2 Updating the pseudo mean flow

For steady flow solutions, i.e., when time marching to a steady state, the pseudo mean flow may be updated as the calculation proceeds. Suppose the residues of the Euler equations have been reduced to a certain level at t=t'. Then, at t=t', let

$$\tilde{U}_{new} = \tilde{U} + u_1 + u_2,$$
 (32.1)

$$\tilde{V}_{new} = \tilde{V} + v_1 + v_2 \,, \tag{32.2}$$

$$\tilde{P}_{new} = \tilde{P} + p_1 + p_2,$$
 (32.3)

$$\tilde{\rho}_{new} = \tilde{\rho} + \rho_1 + \rho_2 \,, \tag{32.4}$$

and, subsequently,

$$u_1 = u_2 = v_1 = v_2 = p_1 = p_2 = \rho_1 = \rho_2 = 0.$$
 (32.5)

This will bring the residues of the PML equations, (31.1)-(31.8), to zero immediately. The time marching may be resumed after this update.

5. Numerical Results

In this section, we present numerical examples applying the PML equations given in previous sections. As pointed out before, it is quite straightforward to implement the PML equations in finite difference schemes since the spatial derivatives involve only the sum of the split variables. In our examples, a 4th-order 7-point explicit central difference scheme has been used for the spatial discretization [8]. For boundary grids where the central difference scheme can not be applied, backward difference schemes of ref [15] are used. Time integration is carried out by a 4th-order Low-Dissipation and Low-Dispersion Runge-Kutta (LDDRK) scheme [14]. In particular, the optimized 5-6 (multi-stage) LDDRK scheme is used. Specifically, for a time step with p stages, the solution is advanced from $t=t_n$ to $t=t_n+\Delta t$ as follows:

1. For
$$i = 1, ..., p$$
, compute

$$\mathbf{K}_{i} = \Delta t F(\mathbf{U}^{n} + \bar{\beta}_{i} \mathbf{K}_{i-1}). \tag{33.1}$$

$$\mathbf{U}^{n+1} = \mathbf{U}^n + \mathbf{K}_p \,. \tag{33.2}$$

The details are referred to ref [14]. Moreover, since an absorption term has been introduced in PML equations, additional stability condition is required in determining the proper time step. Details are given in the Appendix.

In addition, we note that, according to Fourier analysis [16], a central difference scheme can only resolve a limited range of long waves. It is desirable that the short wave components be eliminated or damped in computation. In examples presented here, numerical filtering has been utilized to filter the short waves. In particular, a 10th order numerical filter is applied every 10 time steps. The numerical filter has been designed to reduce only the amplitude of short waves that are not resolved by the central difference schemes. The details are given in the Appendix. The use of filter also reduces the numerical instability encountered with backward differences at boundary grids.

Three examples will be presented below. The first two deal with non-uniform mean flows of a mixing layer and a source/sink flow, respectively. The third example tests the non-linear PML equations where the steady flow generated by a mass source and a time-dependent flow by a small acoustic perturbation are computed directly from the non-linear Euler equations.

5.1 Mixing Layer

The linearized Euler equations (27.1)-(27.4) are solved with a parallel mean flow whose velocity profile is given as follows:

$$\bar{U} = \frac{1}{2} \left[(U_1 + U_2) + (U_1 - U_2) \tanh(y/\delta_{\omega}) \right]$$
 (34)

For the present calculations, $U_1=0.6$ and $U_2=0.2$ (non-dimensionalized by the speed of sound of the upper stream). The mean pressure is constant and the mean density profile is obtained using Crocco's relation in which the temperature is held the same for the two streams [17]. The mixing layer vorticity thickness, δ_{ω} , is taken to be $5\Delta y$.

The parallel shear layer supports the Kelvin-Helmholtz instability wave. The instability wave grows exponentially as it propagates downstream. The linear instability wave solution can be found by solving the compressible Rayleigh equation [17]. At the out-flow, the mean velocity and density are non-uniform. The purpose of this example is to demonstrate the validity of the PML equations proposed in Section 3.

The interior computational domain, where the Euler equations (27.1)-(27.4) are applied, is $[0,200] \times [-40,40]$ with $\Delta x=2$ and $\Delta y=1$. Eigenfunctions of the Kelvin-Helmholtz instability wave are forced at the inflow at x=0 for u', v', p' and ρ' . The chosen non-dimensional frequency

is $\omega = 0.035$, which corresponds to the maximum spatial growth rate. At the out-flow boundary x = 200 and radiation boundaries $y = \pm 40$, absorbing PML domains are applied using equations (27.1)-(27.8). The use of PML equations leads to very little reflection of the out-going disturbances, including the transient fluctuations. Shown in Figure 4 are the instantaneous u-velocity and pressure contours in which PML domains of 10 grid points have been used in the computation. For clarity, the contours in the PML domains are not shown. Comparisons of the numerical solution with linear instability wave solution are shown in Figure 5 for the u-velocity and the pressure as a function of y at x = 194. Very good agreement is found. The amplitude of the u-velocity along the centerline y = 0is also shown in Figure 6, exhibiting an exponential growth. It agrees very well with the spatial growth rate predicted by the linear stability theory, shown as the solid line.

To further demonstrate the effectiveness of the PML equations, a numerical reflection coefficient is computed. This is obtained by comparing the numerical solution with a reference solution. The reference solution is obtained by repeating the computation using the same spatial grid and time step sizes but a larger computational domain so that its solution is not affected by the numerical boundary conditions. The difference between the two solutions has been computed along the vertical line x = 194 near the exit. This measures the reflected waves of the out-flow boundary. The maximum pressure difference as a function of time is shown in Figure 7 for the employed PML domains of width 8, 10, 16 and 20 grid points, respectively. The differences have been scaled by the maximum amplitude of the pressure. With 10 points in the PML domain, the reflection is less than 0.03% and decreases as the width of the absorbing domain increases.

5.2 Acoustic wave in a source/sink flow

The second example for the PML equations of non-uniform mean flow is to compute the acoustic waves in source and sink flows. The mean flow is generated by a mass source/sink as that given in ref [9]. Here the source/sink is centered at (x, y) = (-20, 0). Specifically, the source term in the continuity equation is of the form

$$\bar{S}(x,y) = \begin{cases} -q, & r < r_0 \\ -qe^{-(\ln 2)(r-r_0)^2/36}, & r > r_0 \end{cases}$$
 (35)

where $r = \sqrt{(x+20)^2 + y^2}$. For the source flow, values of q = -0.569 and $r_0 = 10$ have been taken which give a mass flux (outward) of 50 from the source region. The computational domain for the linearized Euler equations is $[-50, 50] \times [-50, 50]$ with $\Delta x = \Delta y = 1$. The mean flow is non-uniform at all four boundaries. The mean velocity field is as shown in Figure 8.

The acoustic wave is generated by adding source terms to the linearized Euler equations (27.1)-(27.4). Specifically,

the linearized terms of $-uS/\rho$, $-vS/\rho$, $\gamma pS/\rho$ and S are added to the right hand sides of (27.1)-(27.4), respectively. Here $S = \bar{S} + s'$ and s' is given as follows:

$$s'(x, y, t) = 0.5e^{-(\ln 2)r^2/9}\cos(\omega t)$$
 (36)

where $r = \sqrt{(x+20)^2 + y^2}$.

Figure 9 shows the instantaneous pressure contours for frequency $\omega=1$. For this calculation, the PML domains have a width of 10 grid points. A comparison with the exact (closed form) solution along y=0 is shown in Figure 10. Excellent agreement is found. The proposed PML equations work just as well for a lower frequency $\omega=0.2$, as shown in Figure 11. This demonstrates that the effectiveness of the PML equations is not affected by variations in wave frequency or wavelength, as pointed out in Section 2. The numerical reflection coefficients are shown in Figure 12 for $\omega=0.2$.

Similar calculations have been carried out for a sink flow, with values of q=0.569 and $r_0=10$ in (35) for the mean flow. This yields a mass flux of 50 into the source region, giving four in-flow boundaries. Figure 13 shows the density variation along y=0 and its comparison with the exact solution. For this calculation, $\omega=0.6$. Again, good agreement is found.

5.3 Steady flow of non-linear Euler equations

In this example, we first compute the steady flow generated by a mass source by solving the non-linear Euler equations directly. Then, a small acoustic perturbation is added to the non-linear equations, similar to the calculations performed in ref [9]. The purpose of this example is to test the non-linear PML equations given in (31.1)-(31.8).

For the steady flow, we solve equations (29.1)-(29.4) in Section 4 where the right hand sides will be modified to be $-u\bar{S}/\rho$, $-v\bar{S}/\rho$, $\gamma p\bar{S}/\rho$ and \bar{S} for the four equations, respectively. The mass source function \bar{S} is as given in (35), with q=-0.569, r0=10 but centered at (x,y)=(-40,0).

To apply the PML equations (31.1)-(31.8), a pseudo mean flow has to be chosen for the PML domains. Since all the four sides will be out-flow boundaries in the present problem, we choose the pseudo mean flow to be the steady flow of a point source located at x=y=0. Such a steady flow can be obtained in a simple way. The details are given in the Appendix (A value of Q=1 has been used). We emphasize that this pseudo mean flow is independent of the specifics of the problem, such as the total flux, the center of the source, etc.

The computational domain is $[-100, 100] \times [-60, 60]$ with PML domains of 20 grid points at four sides and $\Delta x = \Delta y = 1$. Thus the interior domain where the nonlinear Euler equations are applied is $[-80, 80] \times [-40, 40]$. It is found that PML domains larger than those in the linear problems are needed in this example. Values of

 $\beta = 4$ and $\sigma_m \Delta x = 2$ have been used for the variation of absorption coefficients. The variables in the interior domain are initialized as follows:

at
$$t = 0$$
, $u = v = 0$, $\rho = 1$, $p = \frac{1}{\gamma}$.

The variables in the PML domains are all set to be zero initially. The maximum residue of the four equations as a function of time is shown in Figure 14. The residues decrease very quickly, indicating that the transient flow is leaving the computational domain with little reflection. The convergence, however, is slowed when the residues have reached the level of the discretization error, of order 10^{-5} . Figure 15 and 16 shows the time evolutions of the density and u-velocity distributions along y = 0. It is seen, indeed, that the transient fluctuations are leaving the boundaries with very little reflection. Figure 17 and 18 shows the density and velocity profiles along y = 0 as functions of x after 2000 time steps. Also shown are the exact solutions. Very good agreement is observed.

We next compute the time-dependent flow when a small acoustic perturbation is added to the steady flow just obtained. The acoustic forcing will be introduced by modifying the source terms. Specifically, the right hand sides of equations (29.1)-(29.4) are now $-uS/\rho$, $-vS/\rho$, $\gamma pS/\rho$ and S, respectively, where $S = \bar{S} + s'$. The form of s' is as given in (36) with the amplitude now being 10^{-8} .

To capture the minute acoustic disturbances, the residues of the steady flow solution will be first brought to zero to eliminate the numerical noise. Thus, before the acoustic forcing is initiated, the pseudo mean flow is updated as described by (32). This brings down the residues of the PML equations to zero immediately. Then, the canceling-the-residue technique of ref [9] is applied to the Euler equations in the interior domain. This is to add the residue of each equation to its right hand side but with an opposite sign. In this way, the residues of the Euler equations are also brought to zero immediately. Finally, since this steady solution is to be "preserved", the numerical filtering will be applied, at each time step, to the intermediate stage variables of the Runge-Kutta scheme, namely \mathbf{K}_p in (33), rather than to the solution variables.

Figure 19 shows the density fluctuation at two chosen locations as a function of time. The acoustic forcing is started at t=0 in these plots. For this calculation, $\omega=1.0$. Plotted are $\rho-\rho_{steady}$ where ρ_{steady} is the value of the steady solution. It is seen that fluctuations are periodic in time after a transient interval. Since the two chosen locations, $(x,y)=(\pm 70,0)$, are close to the PML domains, this indicates that the acoustic waves are exiting the interior domain with very little reflection. Instantaneous density distribution at t=200 along y=0 is shown in Figure 20, which agrees very well with the exact solution. This example, hence, demonstrates that it is possible to apply the PML equations (31.1)-(31.8) with highly accurate results even when the exact mean flow is not available.

6. Concluding Remarks

A Perfectly Absorbing Technique (PAT) is proposed for numerical solutions of the Euler equations. Perfectly Matched Layer equations have been constructed for linear as well as non-linear Euler equations as an absorbing boundary condition. Plane wave solutions to the PML equations are developed for a uniform flow in an arbitrary direction. It is shown that the proposed PML equations are reflectionless (theoretically) for out-going acoustic, vorticity and entropy waves for any angle of incidence and frequency of the Numerical absorption factors are also estimated. The effectiveness of the absorbing boundary conditions is shown to be independent of the wave frequency/wavelength. Moreover, by introducing a "pseudo mean flow". PML equations for non-linear Euler equations are constructed. They can be applied without the exact mean flow being available at the boundary. Finally, the effectiveness of the proposed PML equations have been demonstrated by numerical examples.

The PML equations have been presented here with the Euler equations being written in primitive variables. In a recent work, the current technique has been extended to equations written in conservation form and to axisymmetric calculations as well [18]. Compared with numerical boundary conditions based on the characteristics or asymptotic solutions, the Perfectly Absorbing Technique employs more equations at the boundary. However, the present technique applies to both the radiation and out-flow boundaries and to both the linear and non-linear out-going waves. It is not necessary to apply the proposed absorbing conditions at a far field. The PML equations also apply where an asymptotic solution is not available. Thus it is a more general technique. Numerical results indicate that it is also a highly accurate technique. As such, it is especially suitable for time accurate calculations such as those in computational aeroacoustics.

Appendix

A. Numerical Stability

Introduction of absorption coefficients in the PML equations warrants additional stability consideration in choosing the time step for a given time integration scheme. Consider convective wave equation modified by an absorption coefficient σ :

$$\frac{\partial f}{\partial t} + c \frac{\partial f}{\partial x} + \sigma f = 0 \tag{A1}$$

where c denotes the wave speed. Using Fourier analysis [16], the semi-discrete equation yields

$$\frac{\partial \tilde{f}}{\partial t} + ick^* \tilde{f} + \sigma \tilde{f} = 0 \tag{A2}$$

where \tilde{f} is the spatial Fourier transform of f and k^* is the effective wave number of the central difference scheme used in the spatial discretization [14]. For numerical stability, the time step Δt should be chosen such that $\lambda \Delta t$, where λ is the eigenvalue of the semi-discrete equation, is within the stability limit of the time integration scheme.

Let the stability boundary of the time integration scheme, e.g., the Runge-Kutta scheme, be denoted as

$$\lambda_r \Delta t = -S(\lambda_i \Delta t) \tag{A1.3}$$

where λ_r and λ_i are the real and imaginary parts of λ , as shown in Figure 21. For equation (A2), we have $\lambda = -ick^* - \sigma$. Then, it follows that, for numerical stability, we need

$$\sigma \Delta t \le S(c \, k_{max}^* \Delta t) \tag{A1.4}$$

where k_{max}^* is the maximum effective wave number. This gives an additional condition for the time step Δt , or conversely, a restriction on the maximum value of σ allowed.

B. Numerical Filtering

Consider a numerical filtering process

$$\bar{f}_i = f_i - \sum_{\ell=-N}^{N} d_{\ell} f_{i+\ell}$$
 (B1)

where f_i is the value of the original function on a grid with uniform spacing of Δx and \bar{f}_i is that of the filtered function. The above can be regarded as a special case of the continuous relation

$$\bar{f}(x) = f(x) - \sum_{\ell=-N}^{N} d_{\ell} f(x + \ell \Delta x).$$
 (B2)

Applying a Fourier transform to the above equation on both sides, we obtain

$$\bar{\tilde{f}}(k) = \left(1 - \sum_{\ell = -N}^{N} d_{\ell} e^{i\ell k \Delta x}\right) \tilde{f}(k) \tag{B3}$$

where \tilde{f} and \tilde{f} are the Fourier transforms of f and \bar{f} , respectively.

The function inside the parentheses of (B3) represents the modification to the amplitude for wave number k. It is desirable that the numerical filtering reduces only the amplitude of the short waves (with large k) that are not resolved in the finite difference scheme. In this paper, we have chosen the coefficients d_{ℓ} such that

$$1 - \sum_{\ell=-N}^{N} d_{\ell} e^{i\ell k \Delta x} = 1 - \sin^{n} \left(\frac{k \Delta x}{2}\right)$$
 (B4)

where n is the order of the filter. It yields exactly N=n/2 and $d_{\ell}=d_{-\ell}$. For n=6, 8, 10, we have

$$\begin{split} n=6,\,N=3,d_0&=\frac{5}{16},d_1=-\frac{15}{64},d_2=\frac{3}{32},\\ d_3&=-\frac{1}{64}\,.\\ n=8,\,N=4,d_0&=\frac{35}{128},d_1=-\frac{7}{32},d_2=\frac{7}{64},\\ d_3&=-\frac{1}{32},d_4=\frac{1}{256}\,.\\ n=10,\,N=5,d_0&=\frac{63}{512},d_1=-\frac{105}{512},d_2=\frac{15}{128},\\ d_3&=-\frac{45}{1024},d_4=\frac{5}{512},d_5=-\frac{1}{1024}\,. \end{split}$$

It is, of course, also possible to further optimize these coefficients. In the present calculations, the 10th order filter has been used in all the examples. For grid points near the boundary where the central stencil does not apply, an "odd" extrapolation of function is carried out for simplicity. Specifically, if x=0 is the left boundary, we use

$$f(x) = 2f(0) - f(-x)$$

for x < 0.

C. Point Source/Sink Flow

We consider the steady flow due to a point source located at (x, y) = (0, 0). In polar coordinates (r, θ) , the solution depends on r along. Thus, by the continuity equation, we have

$$\rho u_r r = Q \tag{C1}$$

where u_r is the radial velocity and $2\pi Q$ is the total mass flux (source flow if Q > 0 and sink flow if Q < 0). Applying the momentum equation in the radial direction

$$\frac{1}{r}\frac{\partial}{\partial r}\left(\rho u_r^2 r\right) + \frac{\partial p}{\partial r} = 0, \tag{C2}$$

and the isentropic relation

$$p = \frac{1}{\gamma} \rho^{\gamma}, \tag{C3}$$

an ordinary differential equation is obtained for ρ :

$$\left(\rho^{\gamma} - \frac{Q^2}{\rho r^2}\right) \frac{d\rho}{dr} - \frac{Q^2}{r^3} = 0 \tag{C4}$$

(Here, variables have been non-dimensionalized by a_{∞} ρ_{∞} and $\rho_{\infty}a_{\infty}^2$ for the velocity, density and pressure, respectively.)

From (C4), it is easy to find that the asymptotic form of ρ for r large is

$$\rho \approx 1 - \frac{Q^2}{2r^2} \qquad \text{for } r \to \infty.$$

Thus ρ can be found by integrating (C4) numerically using (C5) as the starting value for a large r. Alternatively, (C5) can also be used as an approximate solution for ρ at boundary. Once ρ is found, u_r and p can be determined by (C1) and (C3), respectively.

Acknowledgment

This work was supported by the National Aeronautics and Space Administration under NASA contract NAS1-19480 while the author was in the residence at the Institute for Computer Application in Science and Engineering, NASA Langley Research Center, VA 23665, USA.

References

- F. Q. Hu, "On absorbing boundary conditions for linearized Euler equations by a Perfectly Matched Layer", ICASE Report 95-70, 1995. Submitted to Journal of computational Physics.
- 2. J-P Berenger, "A perfectly matched layer for the absorption of electromagnetic waves", Journal of computational Physics, 114, 185-200, 1994.
- 3. K. W. Thompson, "Time-dependent boundary conditions for hyperbolic systems", Journal of Computational Physics, 68, 1-24, 1987.
- Giles, M. B. "Non-reflecting boundary conditions for Euler equation calculations", AIAA J., 28, 2050-2058, 1990.
- 5. A. Bayliss and Eli Turkel, "Radiation boundary conditions for wave-like equations", Communications on Pure and Applied Mathematics, 33, 708-725, 1980.
- B. Enquist and A. Majda, "Radiation boundary conditions for acoustic and elastic wave calculations", Communications on pure and applied mathematics, 32 (3), 1979.
- T. Hagstrom and S. I. Hariharan, "Accurate boundary conditions for exterior problems in gas dynamics", Math. Computation, 51, 581-597, 1988.
- C. K. W. Tam and J. C. Webb, "Dispersion-Relation-Preserving schemes for computational acoustics", *Journal of Computational Physics*, 107, 262-281, 1993.
- 9. C. K. W. Tam and Z. Dong, "Radiation and outflow boundary conditions for direct computation of acoustic and flow disturbances in a nonuniform mean flow", CEAS/AIAA paper 95-007, 1995.

- 10. D. Givoli, "Non-reflecting boundary conditions", Journal of Computational Physics, 94, 1-29, 1991.
- C. L. Streett and M. G. Macaraeg, "Spectral multidomain for large-scale fluid dynamics simulations", Int. Journal Appl. Numer. Math., 6, 123-139, 1989.
- 12. S. Ta'asan and D. M. Nark, "An absorbing buffer zone technique for acoustic wave propagation", AIAA paper 95-0164, 1995.
- P. M. Morse and K. U. Ingard, Theoretical Acoustics, McGraw-Hill, 1968.
- F. Q. Hu, M. Y. Hussaini and J. L. Manthey, "Low-dissipation and -dispersion Runge-Kutta schemes for computational acoustics", *Journal of Computational Physics*, 124, 177-191, 1996.
- J. Gary, "On boundary conditions for hyperbolic difference schemes", Journal of Computational Physics, 26, 339-351, 1978.
- 16. R. Vichnevetsky and J. B. Bowles, Fourier analysis of numerical approximations of hyperbolic equations, SIAM, 1982.
- F. Q. Hu, "A numerical study of wave propagation in a confined mixing layer by eigenfunction expansions", Physics of Fluids, 5 (6), 1420-1426, 1993.
- 18. M. E. Hayder, F. Q. Hu and M. Y. Hussaini, "To-wards a Perfectly Absorbing Layer as a computational boundary", to appear in Proceedings of 15th International Conference on Numerical Methods in Fluid Dynamics, June 24-28, 1996.

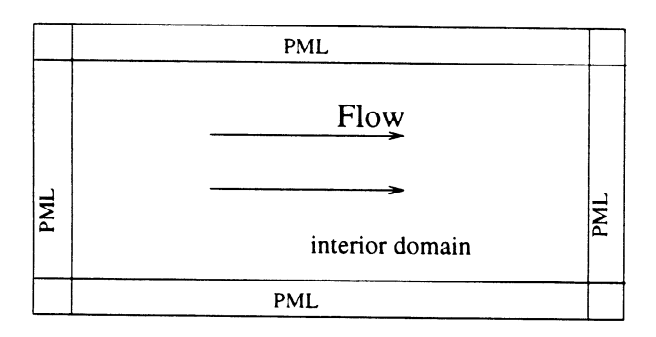


Figure 1. A schematic of the interior and PML domain.

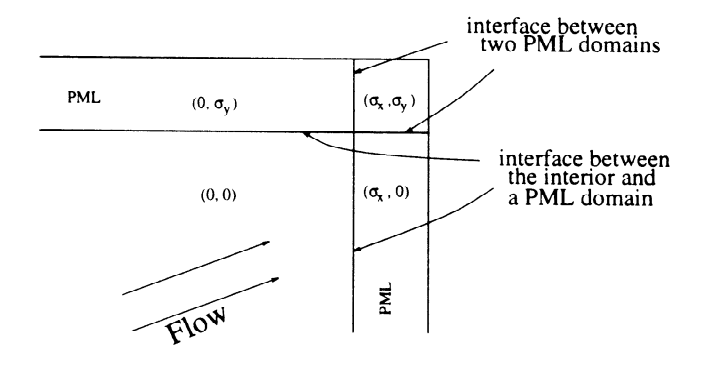


Figure 2. Interfaces and absorption coefficients.

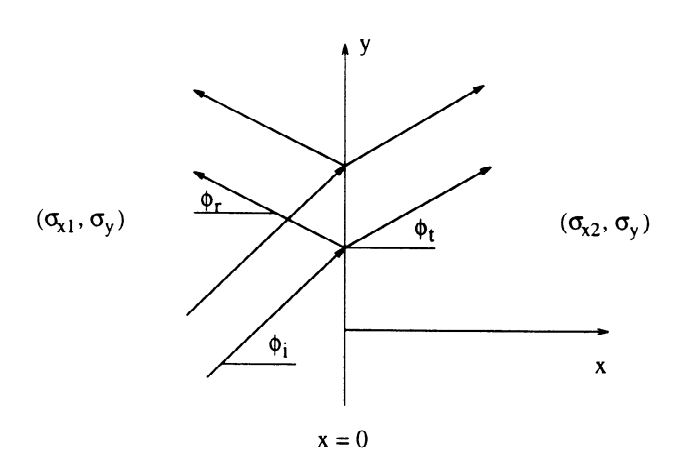


Figure 3. Angles of incident, reflected and transmitted acoustic waves.

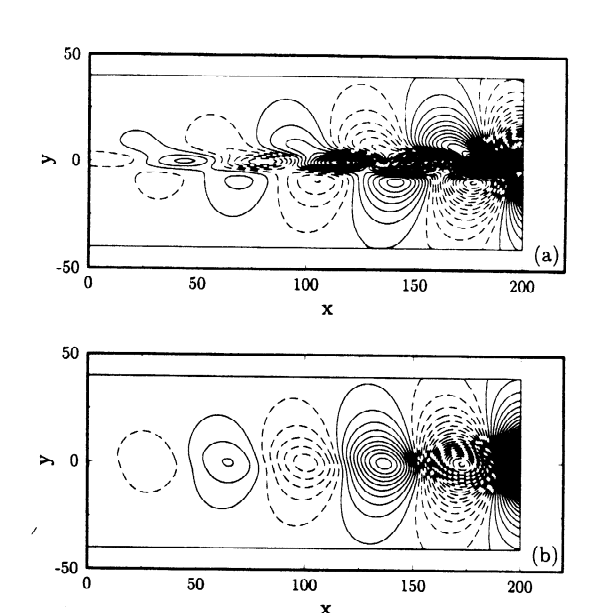


Figure 4. Instantaneous contours of the instability wave. $\Delta x = 2$, $\Delta y = 1$. (a) *u*-velocity, (b) pressure.

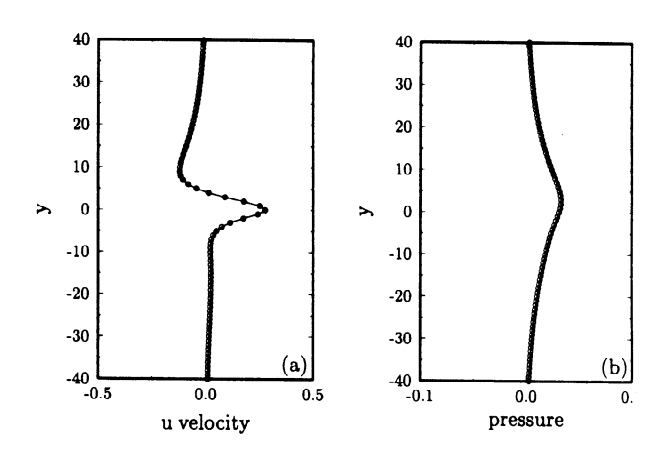


Figure 5. Comparison of the numerical (circle) and linear instability (solid) solutions at x=194 at a given time. (a) u-velocity, (b) pressure.

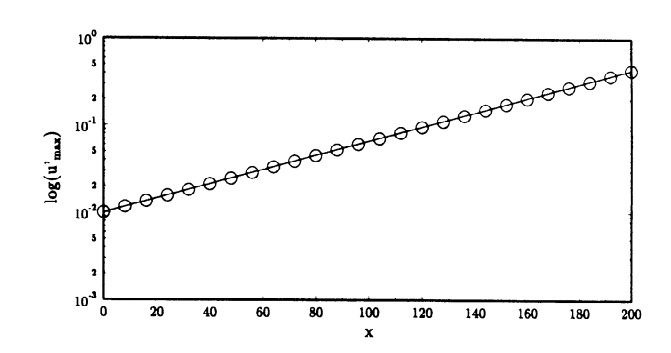


Figure 6. Amplitude of u-velocity along the centerline y=0. The solid line represents the exponential growth rate of the linear instability solution.

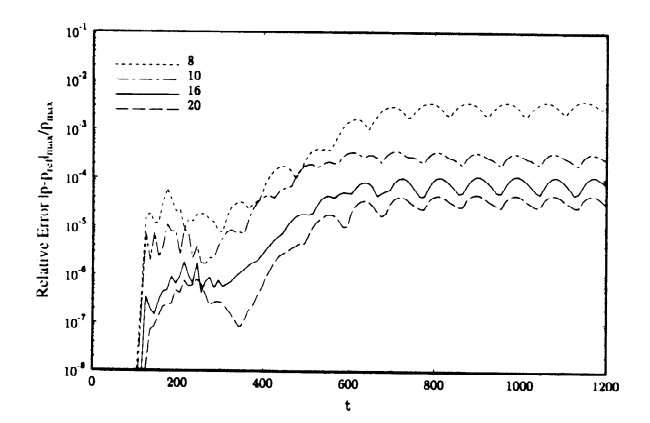


Figure 7. Maximum pressure difference of the computed and reference solutions along x=194. Indicated are the width (grid points) of the PML domains used.

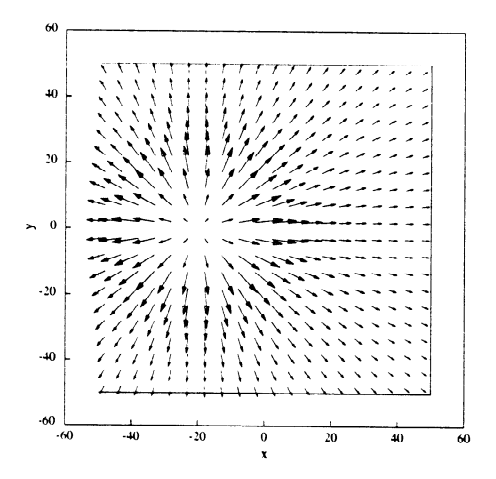


Figure 8. Mean velocity vector field of the source flow, showing non-uniform out-flow boundaries.

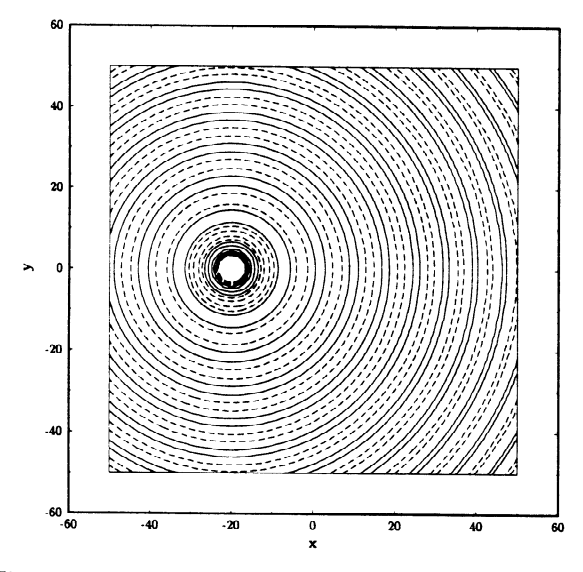


Figure 9. Instantaneous density contours of the computed acoustic wave. $\Delta x = \Delta y = 1$. $\omega = 1.0$. t = 200.

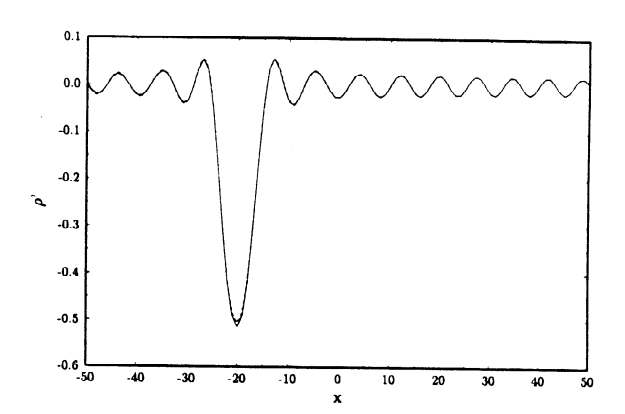


Figure 10. Density variation of the acoustic wave along y=0. $\omega=1.$ numerical, ---- exact.

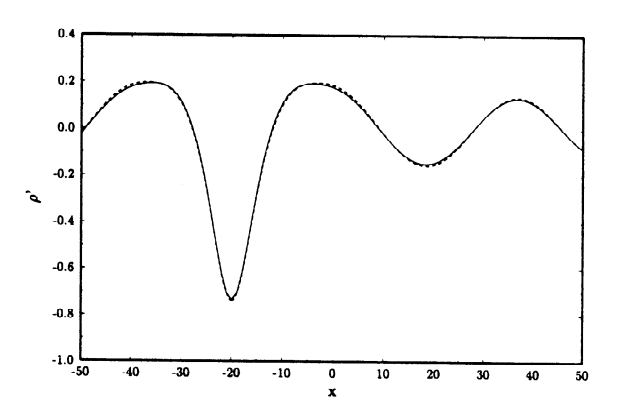


Figure 11. Density variation of the acoustic wave along y=0. $\omega=0.2.$ ———— numerical, ---- exact.

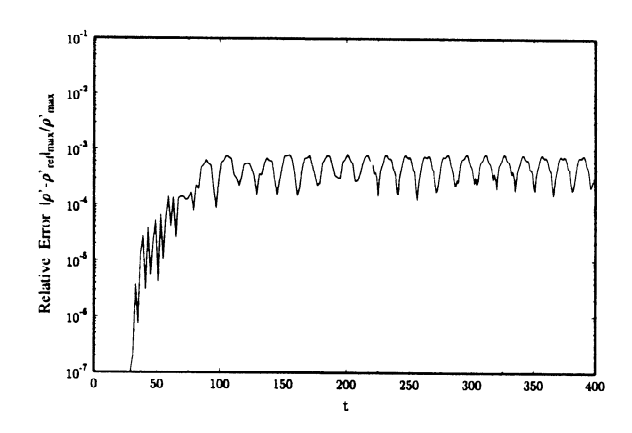
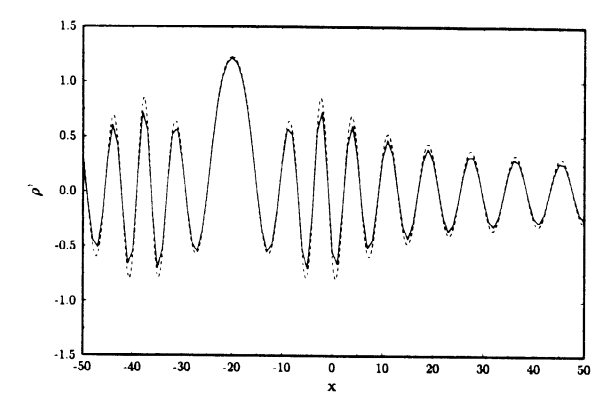


Figure 12. Maximum density difference between the computed and the reference solutions along x = 46. $\omega = 0.2$.



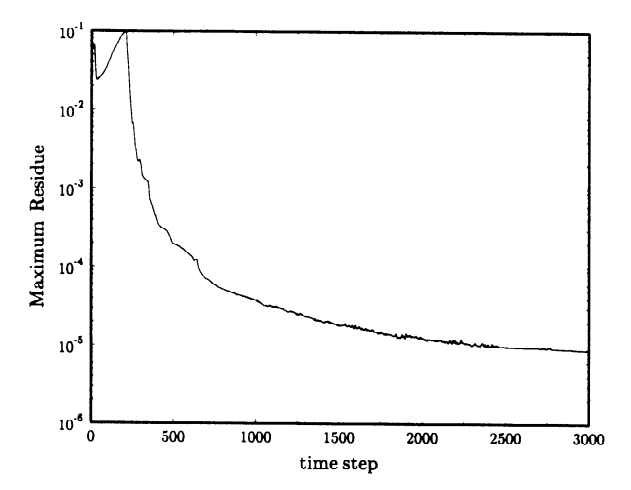


Figure 14. Time history of the maximum residue of the Euler equations.

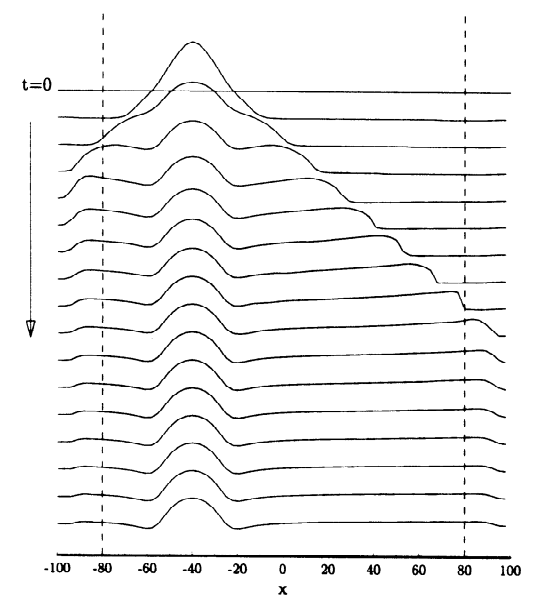


Figure 15. Time evolution of density distribution along y=0. Dotted lines denote the location of PML domains.

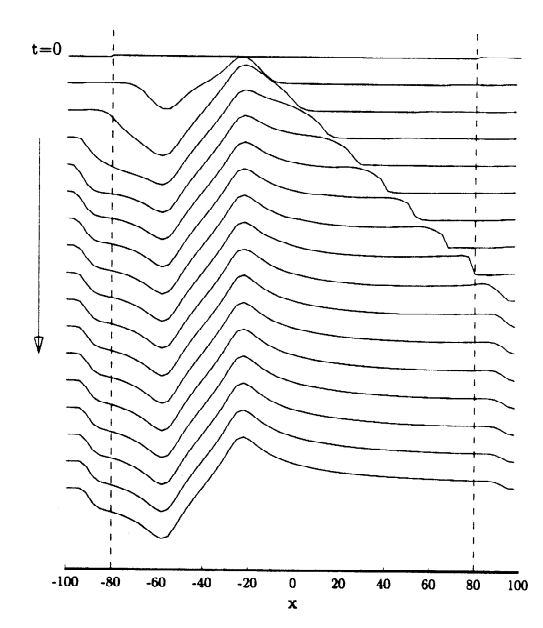


Figure 16. Time evolution of u-velocity distribution along y=0. Dotted lines denote the location of PML domains.

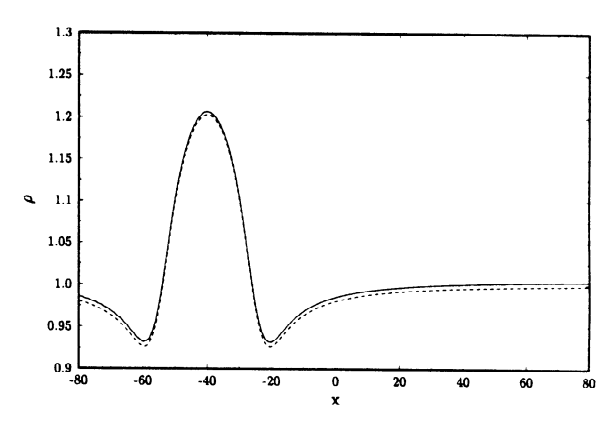


Figure 17. Density distribution along y = 0 after 2000 time steps. ——— numerical, - - - - - exact.

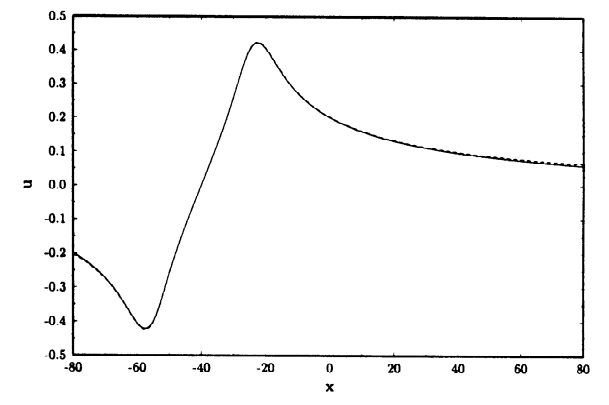


Figure 18. u-velocity distribution along y = 0 after 2000 time steps. —— numerical, - - - - exact.

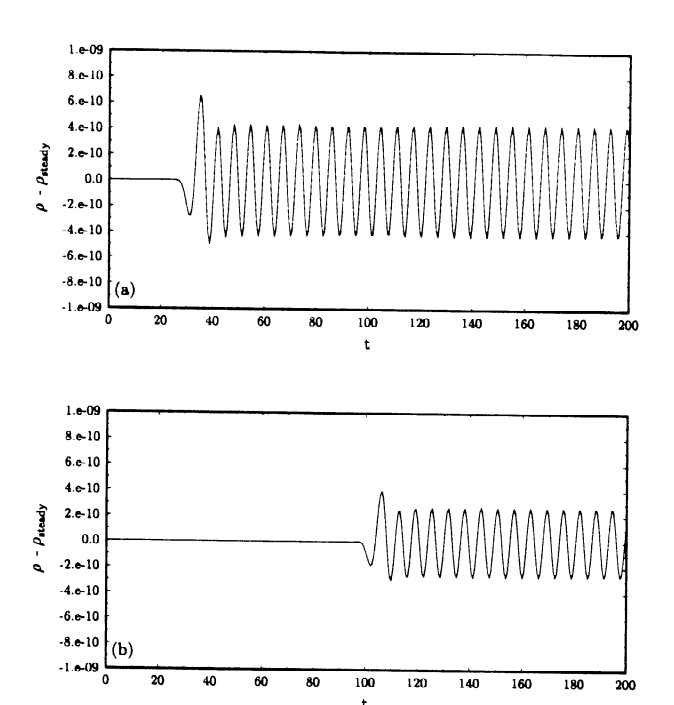


Figure 19. Density fluctuation as a function of time at two locations. (a) (x, y) = (-70, 0), (b) (x, y) = (70, 0).

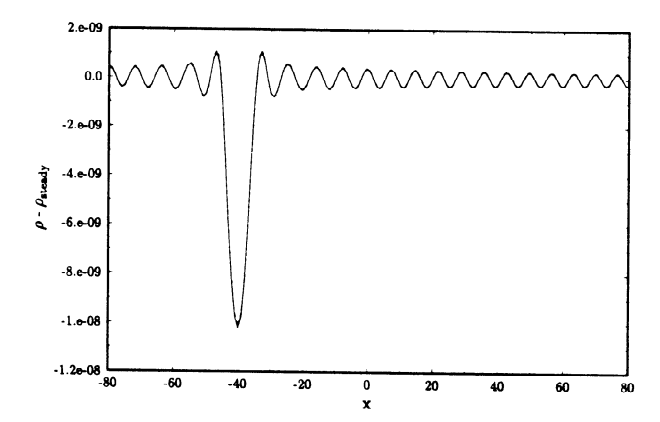


Figure 20. Instantaneous density distribution of the acoustic wave along y=0 computed directly from the non-linear Euler equations. $\omega=1.0,\,t=200.$ numerical, - - - - exact.

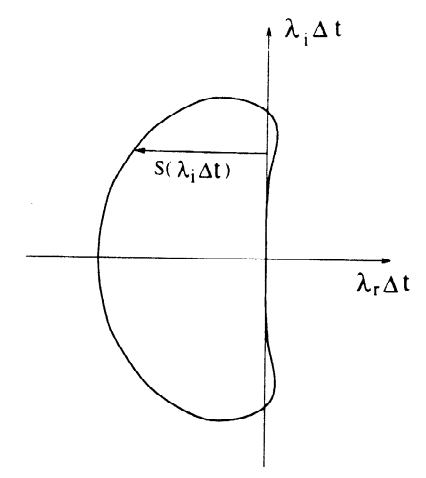


Figure 21. A schematic of the stability limit of a time integration scheme.